Confinement effects on the growth of adsorbates: Interpretation of the formation of monoatomic Ag wires on Pt(997)

F. Picaud, C. Ramseyer, and C. Girardet*
Laboratoire de Physique Moléculaire, UMR CNRS 6624, Faculté des Sciences, La Bouloie, Université de Franche-Comté, 25030 Besançon Cedex, France

P. Jensen
Département de Physique des Matériaux, Université Claude Bernard Lyon-1, 69622 Villeurbanne Cedex, France
(Received 10 November 1999)

Kinetic Monte Carlo simulations based on semiempirical description of metal-metal interactions are developed to interpret recent experiments devoted to the formation of silver wires at the steps of the vicinal Pt(997) surface. The growth mode of Ag on the terraces is discussed as a function of external parameters tied to experimental conditions (coverage, temperature, deposition flux) and of intrinsic parameters characterizing the lateral interactions and the properties of the confined surface through the knowledge of Ag–Ag and Ag–Pt interactions. According to the external conditions, the growth mode is shown to obey a row-by-row plus island process or a fractal island formation at the step, in very good agreement with the data of helium atom scattering and tunneling microscopy.

I. INTRODUCTION

Molecular-beam epitaxy is the most widespread technique to grow materials with desired specification and precision.[1] Most of earlier attempts were devoted to the manufacture of three-dimensional (3D) devices, based on the deposition of alternating layers of different materials, applied to electronics, optics, and catalysis.[2,3] Possible now is the manufacture of lower size metallic objects, like wires or dots,[4–6] grown on metal surfaces, which can exhibit specific electronic[7,8] and magnetic[9] properties, not present in the bulk. However, their fabrication remains a difficult challenge since their size distribution is generally wide due to the random character of the metal atom deposition and diffusion.[10] A lot of experimental effort was paid to define the best conditions for monitoring the diffusion processes that depend on the substrate and adsorbate characteristics. For instance, self-organized growth on substrates exhibiting regularly spaced steps, have been shown to improve considerably the spatial ordering of nanostructures.[11] Heteroepitaxial growth on strain relief pattern has been proved, very recently to be a powerful technique for the formation of highly ordered two-dimensional structures.[12] Indeed, the strain experienced by a thin metal film deposited on a substrate with a different lattice parameter generates dislocations that serve as templates for nanostructure formation. Diffraction techniques such as reflection high-energy electron diffraction or thermal energy helium atom scattering (TEAS) are currently used to control the long-range spatial order of the nanoarrays while scanning tunneling microscopy (STM) probes their local order. In a recent study, self-organized growth of rare gas atoms and metal species (Ag, Cu, Co) on the vicinal Pt(997) surface has been experimentally conducted and probed both by STM and TEAS at grazing incidence.[13] The goal was to fabricate well-ordered and regularly spaced 1D wires by coating the preferential adsorption sites at the steps of the vicinal surface. For the three metals, the authors defined the optimum values of the external parameters governing the diffusion (temperature, coverage and deposition flux) required to tailor 1D arrays along the steps. They found that wire formation is limited, at low temperature, by slow edge diffusion processes and, at high temperature, by heterostep crossing and eventually alloying between the metal adspecies and the substrate. At low coverage and for a deposition flux ranging from 3×10^{-4} ML s^{-1} to 2×10^{-2} ML s^{-1}, nice Ag wires appeared within the temperature range 120 K$\leqslant T\leqslant$550 K, but these wires exhibited higher quality when $T\geqslant$250 K. It has been argued that wire smoothing below 250 K is hindered by edges and corners in Ag islands grown on the terraces, which prevent the Ag adatoms to diffuse towards the step and stick to the 1D array. According to these authors, another path to rearrange the wires could be a possible evaporation/recondensation of the adatoms. The authors also investigated the coverage dependence of the wires and found that smooth one-dimensional wires are present up to 0.5–0.7 ML (monolayer), while the stripes become less perfect and even rough at higher coverage. The roughening of the Ag stripes was interpreted as arising from kinetic or thermodynamic mechanisms. The kinetic argument was that the diffusion of adatoms is directly hindered by their neighbors so that holes in the rows cannot be filled while, from thermodynamics, the relaxation of strains due to the misfit between the Pt surface and Ag layer geometries favors, over a particular coverage threshold, the occurrence of rough structures.

The present paper is an interpretative attempt of the experimental data obtained by the Lausanne group for the wire formation on the vicinal Pt(997) surface. Kinetic Monte Carlo calculations (KMC) are developed on the basis of semiempirical potentials and the results are directly compared to the very recent STM and TEAS experiments of Ag atom growth on Pt(997). Beyond the interpretation of the growth mechanism in terms of diffusion monitored by experimental conditions and by the competition between lateral adsorbate-adsorbate interactions and substrate corrugation

modified by the presence of steps, this comparison serves as a test of the kinetic model and of the interaction potentials.

This paper is organized as follows. Section II is devoted to the presentation of the growth model including its approximations and its limits. The calculations of the energy barriers from the knowledge of the metal-metal interactions are presented in Sec. III. In Sec. IV, the KMC results are compared to the experimental data and the pertinency of the kinetic and potential models is discussed.

II. THE GROWTH MODEL

A good understanding level of the growth properties of metal atoms on metal surfaces has been reached using simple numerical models with a limited number of physical ingredients considered in simulations.[14–17] The DDA model used here takes into account the random deposition (D), diffusion (D), and aggregation (A) mechanisms of atoms on the surface. Even if these latter ingredients are the key processes governing the growth of an adsorbate, the range of situations described adequately by the model is restricted because the experimental conditions can be more complex and require consideration of processes that have been left out in the model. Therefore, in the following we discuss the approximations of the DDA model and its limitations.

A. Geometrical description of the substrate

The geometry of the vicinal Pt(997) surface is shown in Fig. 1. The terraces are closed packed (111) facets with a hexagonal lattice parameter of 2.77 Å, separated by monoatomic $(11\overline{1})$ steps, 2.27 Å in height.[18] The average terrace width is 20.21 Å with a narrow distribution due to step-step repulsive interaction while the terrace length along the step direction is assumed to be infinite and periodic (no step defects).[19] Let us call $\{(l,m)\}$ the set of available adsorption sites for Ag adatoms, where m characterizes an adsorption site belonging to the lth line parallel to the step direction. A terrace is thus defined by the row number $l=1,\ldots,8$ ($l=1$ corresponds to the row closer to the upper step in Fig. 1) and by the intrarow site number $m=1,\ldots,\infty$, since there are 8 rows parallel to the step which contain an infinity of sites. In practice, the maximum value of m is taken equal to 100. We consider that the confined Ag adlayer is in full registry with the Pt terraces so that it forms a (1×1) structure. This assumption appears licit on the basis of previous calculations[20] and experimental findings.[13] Finally, note that the substrate is assumed to be rigid and that no reconstruction or relaxation are taken into account.

B. Deposition

In the simulation, we generate atoms at random (l,m) sites on the surface area A with a flux $F(\theta_d)$ which can be considered as a parameter or directly connected to the experimental deposition time $\tau_F=1/FA$. $F(\theta_d)$ depends on the coverage θ_d of adatoms deposited in τ_F seconds. We limit our study to the monoatomic deposition and we disregard direct deposition of small clusters. Therefore we do not incorporate the possible dissociation of aggregates leading to individual atom redeposition. In addition, we preclude the deposition of particles onto a preexisting island. The simplest scenario would be to assume that when a particle drops on an island, it reaches the border of the island and jumps down to increase the island density. In this paper, we consider reasonably low coverage regimes ($\theta\leqslant0.4$ ML) for which this situation remains uneventful, though such a mechanism could not be disregarded *a priori*. As a consequence, the coverage θ_d that defines the number of atoms in the initial flux is larger than the experimental coverage θ that characterizes the number of atoms that have sticked the surface, referred to the number of available sites on the surface. Finally, note that we do not take into account the kinetic energy of the atoms arriving on the surface and we assume that they experience the potential energy due to the surface, only. All these approximations lead to shifts between theoretical and experimental temperatures. Vvedensky and Clarke[21] have proposed a trick to account partially for this latter effect by depositing the newly arrived atom in a selected site or in a more stable neighbor site in order to speed up the diffusion artificially.

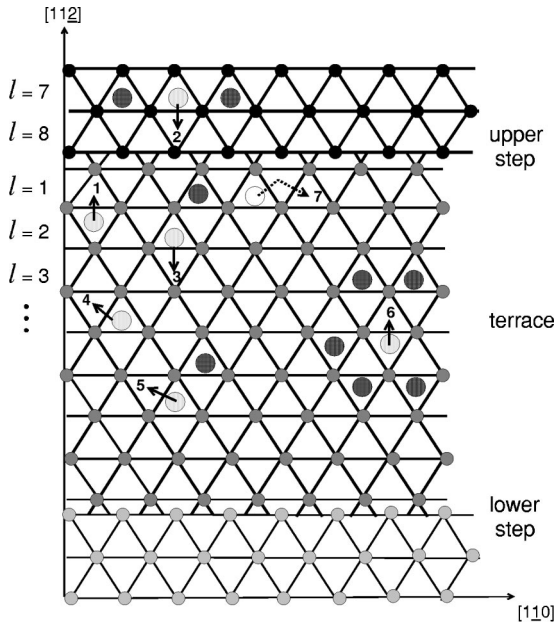

FIG. 1. Top view of the vicinal face (997) of Pt. Small full circles correspond to Pt atoms arranged according to the Pt(111) structure on each terrace. The crystallographic directions are indicated and the row numbering l with respect to a step is also given. Typical diffusion processes ($k=1,\ldots,6$) close to the step (1,2,3) or on the terrace (4,5,6) are schematized; gray circles characterize the moving atoms surrounded by their neighbors (dark circles). The motions are schematized by arrows and the associated energy barriers are listed in Table II. Note that the process 7 is not considered in the model since it corresponds to a jump between nonadjacent wells. But such a process could explain the better ordering of the Ag rows at $T\geqslant250$ K (see the text) and Ref. 37.

C. Diffusion

Many diffusion processes are possible depending on the environment of the implied adatom, namely, on the proximity of the atom from the step that modifies its adsorption properties and from the surrounding atoms that changes its diffusion ability. For a given process k the probability P_k for an atom to jump a barrier at temperature T is given by the

conventional Arrhenius law. Migration of atoms at the surface is modeled within the transition state theory by defining a nearest-neighbor hopping rate as

$$D_k = \nu P_k = \nu \exp\left(-\frac{\Delta E_k}{k_B T}\right), \tag{1}$$

where ΔE_k is the site dependent energy barrier connected to the kth diffusion process, k_B is the Boltzmann constant, and T the substrate temperature. Accurate calculations of the prefactor ν are not available, and the values are rather different depending on the potential shape at equilibrium (second derivative of the potential). Thus, we assume that the adatom center-of-mass trapped in a surface well behaves as a two-dimensional harmonic oscillator with a mean energy $2k_BT$ leading to $\nu = 2k_BT/h$. A diffusion process k is defined as the jump process of an adatom from a well in the lth row with a given configuration of its n nearest- and next-nearest-neighbor adatoms toward an adjacent l'th well with a given final configuration of n' surrounding adatoms. Therefore, k is a function of l,n and l',n', but it does not depend on the site m (or m') in the rows. The values of the energy barriers ΔE_k are determined from the knowledge of the holding and lateral interactions and depend therefore on the potential model (Sec. III, Fig. 2).

At this stage, it should be noted that the number of processes k that can take place on a vicinal surface is so huge that conventional KMC simulations become rapidly cumbersome. Following the algorithm developed by Bortz *et al.*,[22] we have adapted a procedure that speeds up the computational time at low temperature. If n_k is the number of particles that can make the kth process, we define the cumulative probability R_k by

$$R_k = \sum_{i=1}^{k} P_i n_i . \tag{2}$$

After normalizing each probability with respect to the maximum rate $R_{k\,\max}$, a random number r is chosen and the process that satisfies $R_{k-1} < r \leqslant R_k$ is selected. Then one atom is chosen randomly among the n_k atoms, with a uniform probability and it makes the process. Note that when the kth process defined by the energy barrier ΔE_k is degenerated, a random choice of the direction of motion is done for the adparticle. The speed up of the algorithm can be understood by comparing the atom deposition time τ_F on the surface with the time τ_k associated to the kth process, which is given in a first approximation by $\tau_k = h/2kTP_k$. This time characterizes the lifetime of the adsorbate in its adsorption site and thus depends on the temperature. Since τ_k is generally much lower than τ_F, several diffusion motions can proceed between two successive atom deposition events. The loop over the time τ_F is implemented by various steps τ_k. This remark shows that when a process is favorable (short τ_k), the decrease of time $\tau_F - \tau_k$ remains small, while unprobable events (large τ_k) decrease strongly τ_F and tend to force the deposition of another atom. This latter situation occurs inevitably when equilibrium is obtained, i.e., when the probability associated with a process k becomes small, leading to the calculation speed up.

This diffusion model is appropriate for the first stages of growth, roughly until the number of islands on the substrate saturates, since we have disregarded the possibility of dimers, trimers, and larger islands to diffuse. This assumption is licit for epitaxial or quasiepitaxial systems with which we are concerned here since it has been argued that clusters larger than dimers are practically immobile.[17] On the contrary, for nonepitaxial systems such as metal deposition on insulating substrates clusters of more than one hundred atoms can move[23] and this approximation fails. In addition, we consider that the adatoms move in a random direction by one lattice spacing, only. This is a good approximation for temperatures leading to a thermal energy kT smaller than the barrier height but it becomes questionable at temperatures much higher than those studied here. Finally, we consider that the substrate is rigid and disregard the dragging due to the substrate motions.[24,25] As already mentioned, these hypotheses can result in a shift between the calculated and measured characteristics of the diffusion such as temperatures.[26]

D. Aggregation

In the solid on solid and the initial DDA models, when two particles occupied nearest-neighbor sites, they sticked irreversibly. The irreversible aggregation succeeded in reproducing several fractal-like island shapes obtained at low temperature[27,28] especially when edge diffusion of island is hindered. This supposition fails here and, therefore, we have implemented the possible reversible aggregation in the KMC code. Such a reversible aggregation is required to explain the large compacity of islands[29] and the transition from 1D stripes to 2D compact islands for the Ag/Ag(110) and Cu/Cu(110) systems as a function of temperature.[30]

E. Evaporation and exchange

Consideration of evaporation has been shown to affect dramatically the growth kinetics of the film as the temperature increases significantly and to be responsible for totally different island size distributions[31] when the evaporated atoms are reincorporated on the surface. We do not consider the desorption and reincorporation processes since experiments, within the temperature range investigated here, have shown that these phenomena remain negligible.

To summarize, the following parameters, which must be specified in the present simulations, are extrinsic quantities that are issued from experimental conditions, namely, the deposition flux F, the coverage θ, and the substrate temperature T, and intrinsic quantities characterizing the diffusion barriers ΔE_k. The values of the external parameters F, θ, and T are varied in order to reproduce known experimental setups: The temperatures in the simulations range between 100 and 600 K, the coverage does not exceed 0.4 ML, i.e., atoms fill less than half the substrate area A, and the beam flux vary between 10^{-4} and 100 ML s^{-1}. The values of the intrinsic parameters ΔE_k are more difficult to calculate. They are often considered as adjustable parameters. However they are directly connected to the potential characteristics and we can determine their values on the basis of the interaction potential scheme considered here.

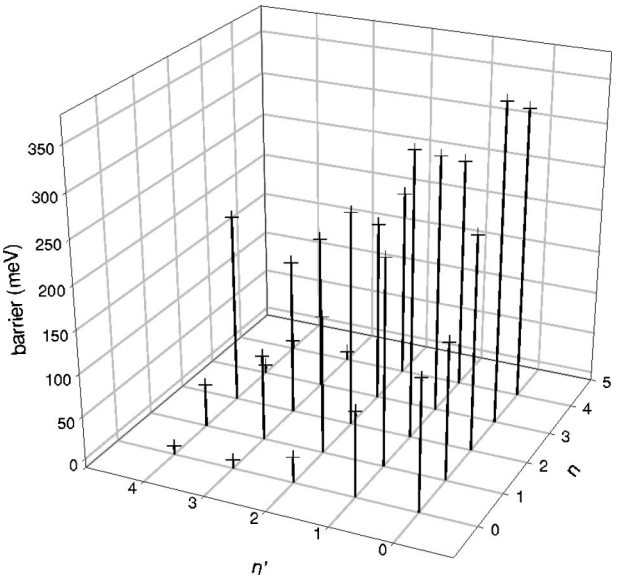

FIG. 2. Plot of the energy barriers (in eV) for the diffusion processes $k\ (l,n,l',n')$ on the Pt terrace vs the number of the diffusing atom nearest neighbors n in the initial state and n' in the final state; $3 \leqslant l \leqslant 7$ and $3 \leqslant l' \leqslant 7$. The maximum number of neighbors is 4.

III. CALCULATIONS OF ENERGY BARRIERS FOR DIFFUSION

A. Potential model

In this section, we calculate the barriers ΔE_k on the basis of potential analysis. We use the semiempirical potential proposed by Rosato *et al.*[32] based on a many-body description of the interactions. This potential has proved to interpret properties of metals depending on the effective width of the electronic density-of-states. It is therefore well suited for transition metals (Pt) exhibiting a large *d* band as well as noble species (Ag). It is expressed as a sum of exponential terms describing the repulsive pairwise contribution and the nonadditive attractive interaction. The potential energy between the *i*th atom and its neighbors *j* located at distances r_{ij} is written as

$$E_i = \lambda \sum_j e^{-p(r_{ij}/r_0 - 1)} - \epsilon \left(\sum_j e^{-2q(r_{ij}/r_0 - 1)} \right)^{\alpha} \text{ with } r_{ij} \leqslant r_c . \tag{3}$$

The values of the nearest-neighbor distance r_0 between metal atoms are 2.77 Å for Pt and 2.89 Å for Ag. The values of the repulsive (λ,p) and attractive (ϵ,q) parameters are determined by fitting the bulk properties of the crystal, namely, the experimental values of the cohesion energy, the bulk modulus, and the elastic constants. The value of the exponent α that describes the many-body nature of the attractive potential is still the subject of controversy.[33] Since in the present situation, we are involved with surface properties, we have thus kept α as a versatile parameter, which allows us to fit accurately both bulk and surface properties of the metal. r_c is a cutoff distance that is limited at the second nearest-neighbor distance between metal atoms to speed up the algorithms ($r_c = r_0\sqrt{2} = 4.08$ Å). Nevertheless, this relatively short value for the cutoff distance can lead to dramatic effects if we do not impose continuity when $r_{ij} > r_c$.[33] Therefore we have ensured the potential continuity at $r_{ij} > r_c$ with a damping exponential function. The values of the parameter set $\{\alpha,p,q,\lambda,\epsilon\}$ have been calculated independently for Ag and Pt metals. For the interaction between heteroatoms (Ag-Pt), the values of the parameter set have been calculated from usual combination rules and their adequacy was tested by directly comparing with available experimental data or *ab initio* calculations.[27] We report the results for Ag-Ag and AgPt interactions in Table I.

TABLE I. Potential parameters [Eq. (1)].

	Ag-Pt	Ag-Ag
λ (eV)	2.4136	1.9994
p	6.5919	6.2177
ϵ (eV)	3.1546	2.5096
q	3.0612	2.9138
α	0.9427	0.9518

B. Calculation of the potential barriers

In a first stage, we determine the equilibrium adsorption site of a single adatom Ag deposited on the vicinal surface and evaluate the holding potential and the corrugation experienced by the adatom. To characterize the diffusion valley we draw the potential map (Fig. 3) obtained by minimizing the interaction energy $E^{\text{Ag-Pt}}$ with respect to the position of the adatom above the substrate. Four main quantities issued from examination of the map and listed in Table II are necessary to model the adsorption of Ag on the stepped surface: The well depth at the stable adsorption site (the hollow site) on a terrace ΔE_T, the corrugation energy ΔE along the diffusion valley, the depth of the adsorption well ΔE_S at the step foot and the Ehrlich–Schwoebel barrier ΔH_S at the step. Table II shows that the ratio $\Delta E_S/\Delta E_T$ is equal to 1.4. This value can be related to the coordination of an adatom, which is about 1.5 greater in the vicinity of a step than on the terrace.

In a second stage, we consider the influence of the lateral interactions. Indeed, the energy barriers associated with an adatom diffusion depend on the holding contribution $E^{\text{Ag-Pt}}$ and on the lateral interactions $E^{\text{Ag-Ag}}$ between the adatom and its neighbors. More precisely, we study the diffusion processes for an atom from the *l*th site and its *n* Ag first nearest neighbors toward the l'th site with n' first nearest neighbors. The processes associated with the same *n* but not with the same next nearest environment have been considered equivalently, their differentiation increases considerably the number of diffusion processes to be listed without contributing significantly to the growth behavior. Moreover, all the processes $k\ (l,n,l',n')$ for which $3 \leqslant l \leqslant 7$ and $3 \leqslant l' \leqslant 7$ are not significantly influenced by the steps and they are all equivalent, while the step influence cannot be disregarded for the processes implying the other rows (l or $l' = 1$, 2, and 8). This leads us to consider 61 diffusion processes. As an example, we have drawn in Fig. 1 some diffusion processes close to or far away from the step and have given in Table II their associated energy barriers. Figure 2 displays energy

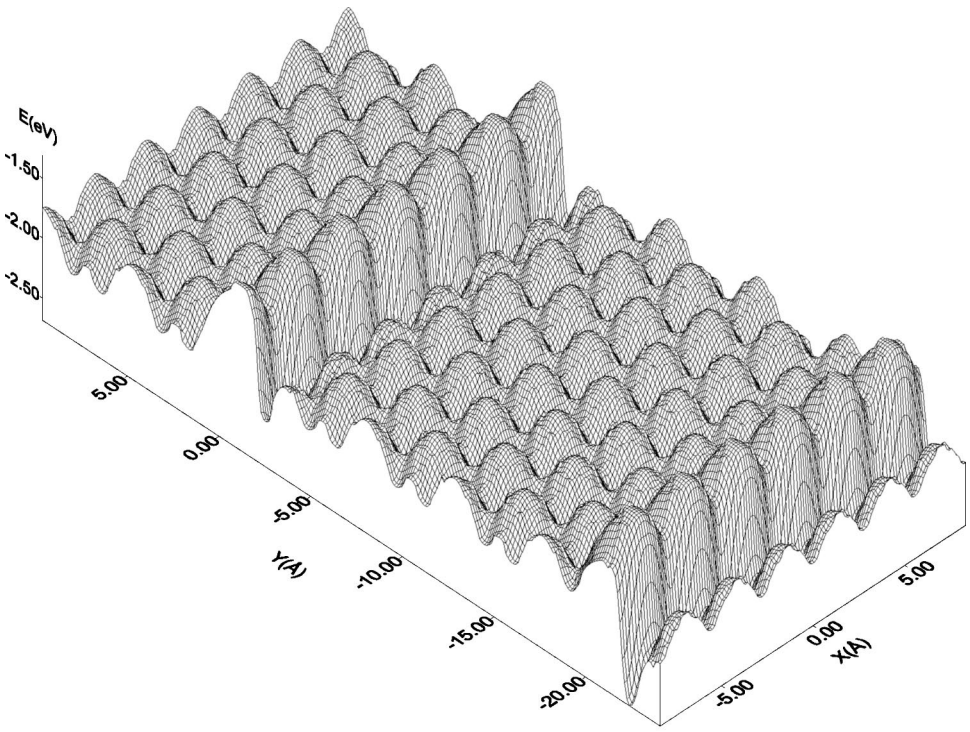

FIG. 3. Potential energy map $E(X,Y)$ for an Ag adatom on the Pt(997) surface; E in eV. See Table II for the corresponding values of the barrier height ΔH_S, the well depths on the terrace ΔE_T and the step ΔE_S, and the corrugation ΔE.

barriers vs the number n and n' of nearest neighbors for all the terrace diffusion processes k (l,n,l',n') with $3 \leqslant l \leqslant 7$ and $3 \leqslant l' \leqslant 7$. We can see that the barrier values vary from a few tens of meV up to more than 0.3 eV. The other processes that are influenced by the step and not given here, have the same behavior with n and n'.

For each investigated process k, the total energy experienced by the adatom has been calculated in the stable site and at the saddle point along the diffusion path in the presence of the surrounding adatoms, and the energy difference ΔE_k at these two points has been evaluated. This is in contrast with the bond breaking model usually considered in growth simulations[34] for which the energy barrier to diffusion is calculated as the result of the holding energy barrier plus a term representing the number of bonds experienced by the adatom. Although this latter model appears crude, it can be used to give some ideas on the nearest-neighbor bond energy value. If we assume that the lateral energy difference in the initial and final configuration of a given process is a function of the number of bonds lost or gained in the diffusion jump, a value of 0.47 eV for the Ag/Ag bond on the Pt surface is estimated with the present potential form.

TABLE II. Adsorption characteristics for an Ag atom above the Pt(997) surface and energy barriers ΔE_k for typical diffusion processes k shown in Fig. 1.

Energy barriers (eV)	Ag/Pt(997)
ΔE_T	2.14
ΔE_S	3.68
ΔE	0.143
ΔH_S	0.39
ΔE_1	0.007
ΔE_2	0.267
ΔE_3	0.177
ΔE_4	0.143
ΔE_5	0.150
ΔE_6	0.200

IV. RESULTS AND COMPARISON WITH EXPERIMENTS

A. Ag wire growth vs coverage

Three markedly different modes of film growth on 3D crystal can be distinguished:[35] The layer by layer growth mode (or Frank–van der Merve), the island growth (or Vollmer–Weber), and the intermediate layer plus island growth mode (or Stanski–Krastanov). Keeping in mind this classification, we can analyze the growth modes in the vicinity of steps, and see the similarities with the 3D approach. This latter growth is guided especially by the competition between the holding and lateral interactions while the present two-dimensional growth is a function of the Ag-Pt step (Fig. 3) and lateral Ag-Ag interactions. In addition a comparison of the results of the present kinetic model can be done with TEAS and STM experiments[13] to test the model and the potential adequacy.

We have determined the site occupation of terraces on the vicinal surface as a function of the coverage θ. The length of a terrace is 50×2.77 Å and the steps settling boundaries are parallel and without defects (no kink, no vacancy). Figure 4 displays the row occupation of silver atoms adsorbed on five similar Pt(997) terraces, at various Ag coverages θ ranging from low coverage ($\theta = 0.1$) to less than half completion ($\theta = 0.35$), at 300 K and for a relatively slow flux (10^{-3} ML s^{-1}). In the inset of Fig. 4, we give the relation between the deposited θ_d and real θ coverages. When $\theta_d \leqslant 0.3$, the portion of atoms that has been deposited on an already occupied site is negligible and we have $\theta \simeq \theta_d$, while for higher coverages ($\theta_d \geqslant 0.35$), the portion of impinging

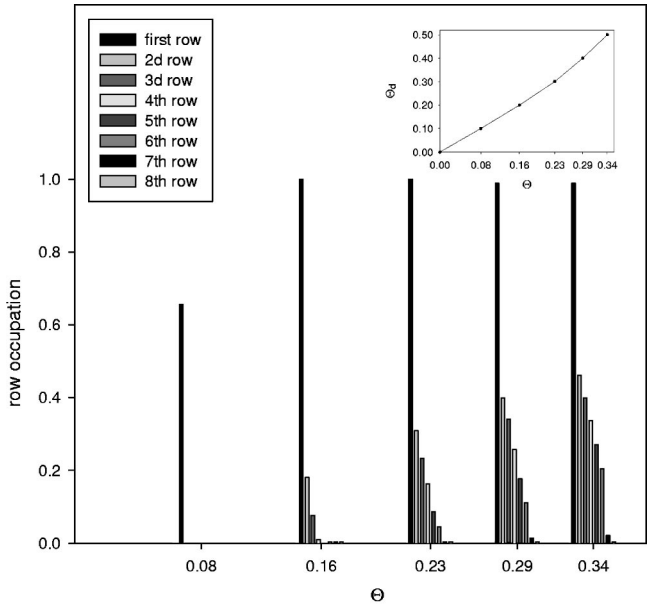

FIG. 4. Ag row occupation on Pt(997) vs coverage θ determined within the KMC simulation at 300 K and for an atom flux equal to 10^{-3} ML s^{-1}. The histogram represents the Ag occupation of the successive rows, from one to eight, created along the step. Unity corresponds to row completion. In the inset, we give the correspondence between the deposited coverage θ_d and the real coverage θ.

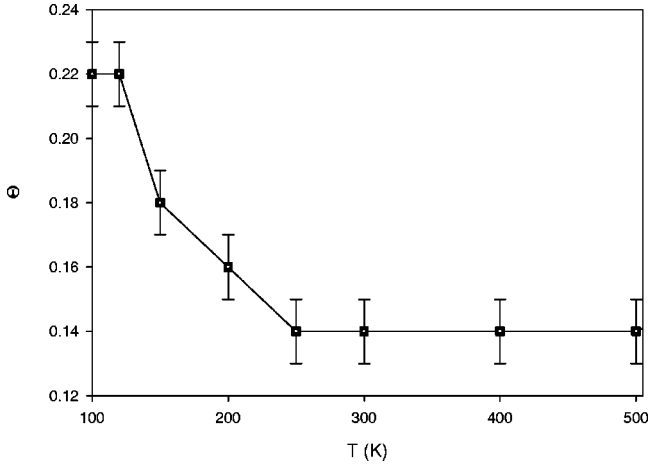

FIG. 5. Ag coverage θ vs temperature T leading to the first row completion. The error bars characterize the uncertainty over the statistical distribution of adatoms. The asymptotic value of θ at high temperature is close to the ideal first row completion ($\theta_1 = 1/8 = 0.125$).

atoms on islands cannot be neglected since the difference between θ_d and θ exceeds 25%. The number of available sites on each terrace is equal to $(M \times L) = (50 \times 8)$ and the statistics is done over ten independent runs. At the ambient temperature, the diffusion is efficient whereas the desorption and exchange processes are very unprobable.

At low coverage ($\theta \leqslant 0.2$), the Ag adatoms tend to coat the step defining the upper terrace and they fill mainly the first row of adsorption sites which saturates at $\theta \simeq 0.16$. This row coating is repeated at all footsteps of the five terraces and regular one-dimensional nanowires occur on the vicinal surface. When coverage increases up to 0.35, the other rows grow simultaneously. However, this growth is not random since the row occupation obeys an exponential decay as a function of the row proximity with respect to the upper step. Even if the row occupation, except the first one, is not complete, we see an ordering with a nearly constant slope for each row population from the second to the sixth. Therefore we can conclude that the Ag/Pt system exhibits a partial row-by-row growth when coverage increases. These results corroborate the data of TEAS experiments[13] obtained at low coverage that predict the occurrence of one or two Ag nanowires parallel to the steps. Aside from the nanowire formation, we want to emphasize that their corresponding distribution is regular and that the vicinal Pt surface acts as a model substrate for the Ag adsorbate. Only small defects like kinks or vacancies, or a narrower distribution of steps could break this nice nanowire grating.

B. Ag wire formation vs temperature

Let us now focus on the row appearance and stability as a function of temperature. In Fig. 5, we show Ag coverage θ vs T leading to the first row completion. At high temperature ($T \geqslant 300$ K), we see that the first row is filled when the coverage θ is slightly larger ($\theta \simeq 0.14$) than the ideal first row completion ($\theta_1 = 1/8 = 0.125$). Most of the adatoms have moved toward the most stable adsorption sites at the bottom of the steps due to a large diffusion energy. The difference between the ideal and observed coverages required for the first row completion comes from the statistics, namely, a few atoms occupy the second row before the completion of the first row is reached. At low temperature (150 K $\leqslant T \leqslant$ 300 K), the coverage θ exceeds in a significant way the completion limit θ_1. A steep decay of the coverage dependence θ occurs at about 200 K. This peculiar behavior is due to a kinetic phenomenon for which the adatoms stick to the second row without having the possibility of reaching the first row. It would be an error to think that this feature is due to a decrease of the atom migration. Indeed, below 300 K the diffusion coefficient of a single Ag adatom does not decrease significantly, and, even if the corrugation of the surface reduces the diffusion at low temperature, the Ag monomers can diffuse on the Pt(111) surface.[36] The row filling has been shown to be efficient even at 100 K.[20] In the light of these results and from a closer examination of snapshots, we can show that the first two rows are preferentially filled although they exhibit holes at low temperatures. This roughening is due to the strength of the lateral Ag-Ag interactions that prevents the adatom detachment from island edges and thus the reorganization of the atom occupation inside the rows.

The occurrence of the first two rows and their shape evolution with T is fully corroborated by STM and TEAS measurements.[13] In addition, the steep decay of the coverage dependence vs temperature is observed experimentally though it appears at a larger temperature (250 K). The shift between the calculated (200 K) and the experimental (250 K) values can have at least two origins. It could be due to interaction potential inaccuracies or to some uncertainties on the values of the deposition flux. To explain the coverage shifts between ideal ($\theta = 0.125$) and observed ($\theta = 0.14$) values at high temperature and between the theoretical ($\theta = 0.22$) and experimental value ($\theta = 0.18$) at low temperature (Fig. 5) we

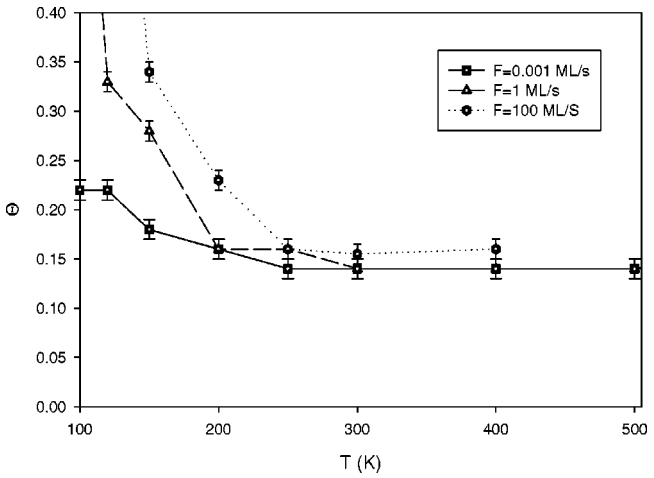

FIG. 6. Ag coverage θ vs temperature T, when the first row is filled, for different flux values ranging from to 10^{-3} to 100 ML s^{-1}.

can invoke other diffusion processes not included in the present KMC simulations. Indeed, let us remind that we have considered thermodynamic processes implying diffusion jump from a stable hollow site to an adjacent similar site throughout potential valleys, only. However, since the rows appear to be well-ordered below 250 K in the experiments, the Ag adatoms could certainly diffuse along other paths to reorganize the rows, such as diffusion along the steps. Indeed, previous molecular-dynamics calculations[37] showed that diffusion along steps of homoepitaxial systems like silver or gold atoms is quasi-one dimensional. This path represented in Fig. 1 connects two stable next-nearest-neighbor step sites along a straight line, in such a way that the diffusive atom crosses a metastable site, located more closely to the step. The consideration of such additional processes would increase the computational time without giving additional physical arguments on the whole behavior of the growth with T.

C. Ag growth vs flux

To complete this discussion, we consider the influence of the atom flux on the growth mechanism. In the previous simulations, the flux value was chosen to be low ($F \simeq 10^{-3}$ ML s^{-1}) in accordance with the conditions generally used in MBE growth.[13] Simulations performed for several values of the flux F ranging between 10^{-4} and 10^{-2} ML s^{-1} (not presented here) show the same behavior of the atom growth on the vicinal Pt(997) surface. At higher flux, the deposition phenomenon first balances and then crushes the diffusion regime. For instance, the sequential atom occupation of the step obtained for Ag at 300 K disappears when the flux is strongly increased ($F \simeq 100$ ML s^{-1}). This behavior is clearly evidenced in Fig. 6. At low temperature ($T \simeq 120$ K), the first Ag row still decorates fully the Pt step but other atoms occupy randomly sites on the terrace but such a completion occurs at much higher coverage ($\theta = 0.35$). The diffusion is hindered and fast deposition prevents the nice step coating observed at lower flux. In addition, the diffusion of deposited atoms is forbidden by the strong flux that favors aggregation of Ag adatoms forming small islands on the terraces. At higher temperature, the diffusion increases but the high deposition still favors aggregation. However the reversible aggregation leads to the bond breaking of islands atoms that can thus participate to the diffusion toward the step. There is a subtle competition between the deposition and diffusion processes and the first row completion is obtained for coverages still slightly larger ($\theta \simeq 0.16$) than θ_1. A further increase of the deposition flux leads to the percolation regime.

The features described previously points out that a careful attention should thus be paid to monitor adequately the row-by-row growth in an out-of-equilibrium process. The range of flux values [$10^{-4} - 10^{-2}$ML s^{-1}], which conducts to a nice coating of the steps, compares very well with the optimal values obtained in experiments.[13]

D. Confinement effects on fractal-like behavior at intermediate coverages

Most of the previous results (Sec. III A) focused on the role of step confinement on the metal-atom growth when diffusion is the efficient process. In this section, we discuss the growth of Ag in the regime of partial hindering of the diffusion at island edges on the vicinal surfaces. To this end, let us briefly remind the results obtained[10] for the Ag growth on the perfect Pt(111) surface (no step) when $T \leqslant 120$ K, on the basis of embedded atom method (EAM) calculations.[27] The Ag island shape was found to be dendritic with three branches corresponding to half the main directions of hexagonal symmetry of the substrate surface while the three other directions are forbidden by diffusion motions due to the presence of step edges.[27] Using the semiempirical potential approach we have done the same simulations in order to test the pertinency of this potential. The calculated diffusion barriers at the island edges are represented schematically in Fig. 7, and they are very similar to those obtained by EAM calculations.[27] As a consequence, the Ag islands (Fig. 8) have the same characteristics (dendritic shape, diameter, fractal dimension, etc.) as those simulated and observed by Bromann.[27] This corroborates the fact that the semiempirical potential used here is particularly well adapted. However, note that the fcc and hcp sites have the same energies in our calculations, leading to equiprobable orientations for the islands, although effective medium theory (EMT) (Ref. 27) calculations have suggested that fcc sites could be more stable by a few tenths of eV, thus favoring one island orientation with respect to the others.

In order to discuss the influence of steps and thus of the atom confinement within this particular growth regime, we compare the results of KMC calculations performed on a quasi-infinite Pt(111) surface containing a single step, with those obtained on the small terraces of the vicinal Pt(997) surface. The Pt(111) surface with one step is modeled by a box containing $(M \times L) = (200 \times 200)$ adsorption sites. For the Pt(997) we use a box with 15 terraces each having $(M \times L) = (120 \times 8)$ available adsorption sites. Figure 8 shows a typical snapshot of the KMC simulation for the single stepped surface that can be directly compared with the STM images obtained by the Lausanne group.[38,39] We see that the island shape is always dendritic but the symmetry breaking of the surface due to the step reduces the number of backbones to one or two, depending on the step orientation. In

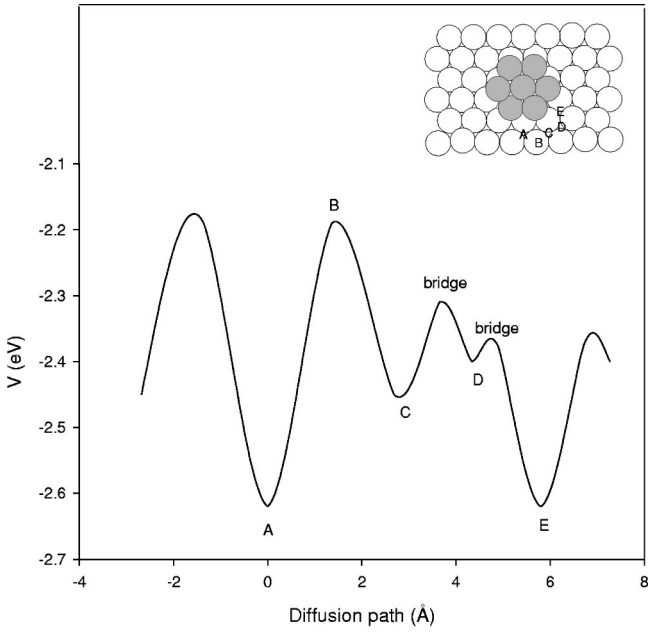

FIG. 7. Calculated energy barriers along the diffusion paths obtained with the potential of Eq. (1) for an Ag adatom along the edge of a hexagonal Ag island (gray circles in inset) adsorbed on the Pt(111) surface (empty circles in inset). The diffusion path is schematized in inset using letters A,B, . . . ,E that correspond to successive adsorption sites.

Fig. 8, the step orientation [100] has been chosen in such a way that one over the three branches disappears, only. A rotation by 60° of the step direction would lead to the occurrence of a single branch perpendicular to the $[1\bar{1}0]$ step. In addition, to the island formation, simulations show a step decoration by one row and then after this decoration we observe that dendritic growth proceeds.

The growth behavior is completely different when Ag adsorbs on small Pt terraces (Fig. 9). The fractal shape of Ag islands disappears and is replaced by more compact islands

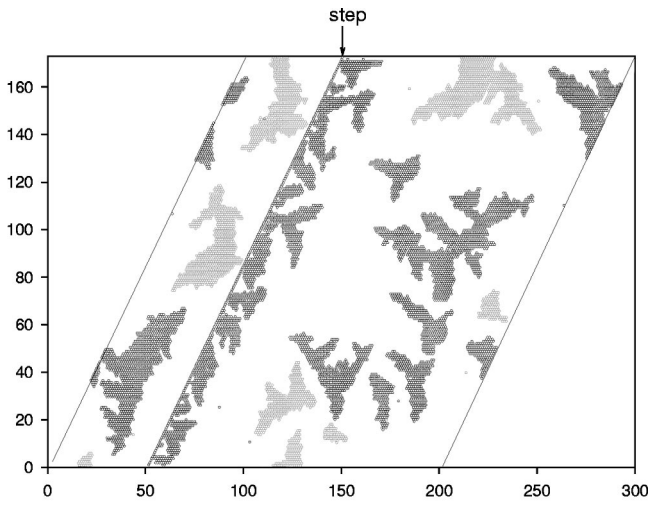

FIG. 8. KMC snapshot obtained on the Pt(111) surface containing (200×200) adsorption sites and one step along the [100] direction at $T=120$ K, $F=10^{-3}$ ML s^{-1}, and $\theta=0.3$. Ag islands exhibit dendritic shape with, however, a reduced number of branches.

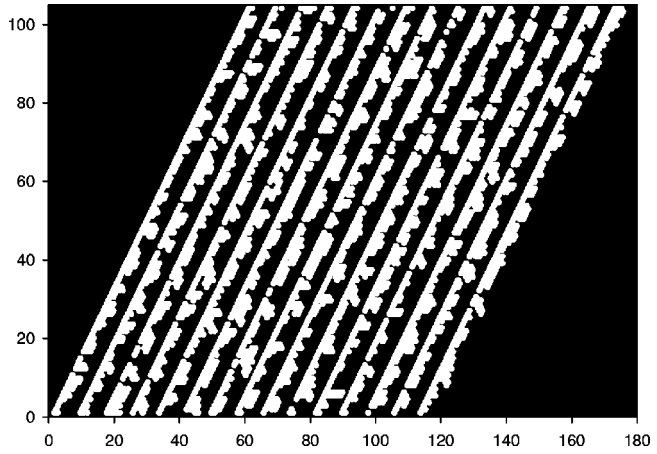

FIG. 9. KMC snapshot obtained on the vicinal Pt(997) surface containing 120×120 adsorption sites and 15 terraces delimited by steps along the $[1\bar{1}0]$ direction at $T=120$ K, $F=10^{-3}$ ML s^{-1}, and $\theta=0.3$. Ag does not exhibit a fractal behavior, and quasi-1D nanostructures are observed close to the steps.

that are attached to the steps with a 1D behavior. In order to compare these results with STM measurements,[13] the snapshot given in Fig. 9 is obtained for $\theta=0.3$. We have schematized the Ag atoms as balls of 6 Å diameter that reproduce the apparent size of the atoms viewed by the STM tip.[40] The comparison with the corresponding figure in the experimental paper[13] is remarkable. At half completion, all the Ag atoms coat the vicinity of the steps to form rough but quasi-1D islands. The repulsive Schwoebel barrier prevents the Ag atoms to descend over their lower step (Fig. 1) and, as a result, diffusion and deposition are restricted at the footsteps. Examination of the internal structure of the small aggregates shows that they are analogous to that observed in experiments, having a shape of drops. This feature indicates that, inside the 1D island, the growth obeys mostly a Stransky-Krastanov mechanism, which is however neutralized by the confinement. As a result, 1D rough islands are formed.

V. CONCLUSION

On the basis of kinetic Monte Carlo calculations using semiempirical potentials to describe the interactions between metal atoms (Pt-Ag and Ag-Ag), we have shown that we can interpret most of the experimental phenomena evidenced by TEAS and STM on the growth of Ag wires and islands on confined terraces of the vicinal Pt(997) surface. The qualitative agreement with experiments regarding the influence of temperature, coverage and deposition flux on the growth mechanisms is remarkable. The remaining small differences between calculations and measurements, especially on the asymptotic first row coverages at high and low temperatures and on the temperature range leading to ideal first row filling should probably be removed by including multijumps diffusion processes and improving the accuracy of some potential parameters. But these effects are clearly an order of magnitude smaller than the phenomena described in this paper.

The calculated flux and temperature ranges required to

fabricate the best wire patterns are fully consistent with the values obtained from experimental considerations for the Ag/Pt systems. Therefore, by improving slightly potentials and jump processes associated with diffusion, it should be possible to invert the problem for other substrates and adsorbates in order to define from simulations the best conditions that should lead to the fabrication of well-shaped 1D nanostructures.

*Electronic address: claude.girardet@univ-fcomte.fr

[1] K. Ploog, in *Crystal Growth, Properties and Applications*, edited by H. C. Freyhardt (Springer-Verlag, Berlin, 1980).
[2] J. E. Houston, C. Peden, D. Blair, and D. Goodman, Surf. Sci. **176**, 427 (1986).
[3] M. Haruta, Catal. Today **66**, 153 (1997).
[4] J. M. Moison, F. Houzay, F. Barthe, F. Leprince, E. André, and O. Vatel, Appl. Phys. Lett. **64**, 196 (1994).
[5] D. Leonard, M. Krishnamurthy, C. M. Reaves, S. P. Denbaars, and P. M. Petroff, Appl. Phys. Lett. **63**, 3203 (1993).
[6] M. Sundaram, S. Chalmers, P. Hopkins, and C. Gossard, Science **254**, 1326 (1991).
[7] Y. Hasegewa and P. Avouris, Phys. Rev. Lett. **71**, 1071 (1993).
[8] F. J. Himpsel and J. E. Ortega, Phys. Rev. B **50**, 4992 (1994).
[9] P. Grünberg, R. Schreiber, Y. Pang, M. B. Brodsky, and H. Sowers, Phys. Rev. Lett. **57**, 2442 (1986).
[10] H. Röder, E. Hahn, H. Brune, J. P. Bucher, and K. Kern, Nature (London) **366**, 141 (1993).
[11] V. Marsico, M. Blanc, K. Kuhnke, and K. Kern, Phys. Rev. Lett. **78**, 94 (1997).
[12] H. Brune, M. Giovannini, K. Broman, and K. Kern, Nature (London) **394**, 451 (1998).
[13] P. Gambardella, M. Blanc, H. Brune, K. Kuhnke, and K. Kern, Phys. Rev. B **61**, 2254 (2000).
[14] J. Weeks, G. Gilmer, and K. Jackson, J. Chem. Phys. **65**, 712 (1976).
[15] P. Melinon, P. Jensen, J. Hu, A. Hoareau, B. Cabaud, M. Treilleux, and D. Guillot, Phys. Rev. B **44**, 12 562 (1991).
[16] P. Meakin, Phys. Rev. Lett. **51**, 1119 (1983).
[17] P. Jensen, A. Barabasi, H. Larralde, S. Havlin, and H. E. Stanley, Phys. Rev. B **50**, 15 316 (1994).
[18] V. E. Marsico, Ph.D. thesis, Ecole Polytechnique Féderale de Lausanne, 1995.
[19] E. Hahn, H. Schief, V. E. Marsico, A. Fricke, and K. Kern, Phys. Rev. Lett. **72**, 3378 (1994).
[20] F. Picaud, V. Pouthier, C. Ramseyer, and C. Girardet, Surf. Rev. Lett. **6**, 669 (1999).
[21] S. Clarke and D. Vvedensky, J. Appl. Phys. **63**, 2272 (1988).
[22] A. B. Bortz, M. H. Kalos, and J. L. Lebowitz, J. Comp. Physiol. **17**, 10 (1975).
[23] I. Furman and O. Biham, Phys. Rev. B **55**, 7917 (1997); C. Henry, C. Chapon, and B. Mutafschief, Thin Solid Films **46**, 157 (1977).
[24] T. Ala-Nisila, J. Kjoll, S. C. Ying, and R. A. Tahir-Kheli, Phys. Rev. B **44**, 2122 (1991).
[25] U. Kurpick, A. Kara, and T. S. Rahman, Phys. Rev. Lett. **78**, 1086 (1997).
[26] M. Dienwiebel, P. Zeppenfeld, J. Einfeld, F. Picaud, C. Ramseyer, and C. Girardet, Surf. Sci. **446**, L113 (2000).
[27] K. Bromann, Ph.D. thesis, Ecole Polytechnique Féderale de Lausanne, 1997.
[28] P. Jensen, A. Barabasi, H. Larralde, S. Havlin, and H. Stanley, Phys. Rev. E **50**, 618 (1994).
[29] C. Ratsch, A. Zangwill, P. Smilauer, and D. Vvedensky, Phys. Rev. Lett. **72**, 3194 (1994).
[30] C. Mottet, R. Ferrando, F. Hontinfinde, and A. C. Levi, Surf. Sci. **417**, 220 (1998).
[31] P. Jensen, H. Larralde, and A. Pimpinelli, Phys. Rev. B **55**, 2556 (1997).
[32] V. Rosato, M. Guiloppe, and B. Legrand, Philos. Mag. A **59**, 321 (1989).
[33] J. Guevara, A. M. Llois, and M. Weissmann, Phys. Rev. B **52**, 11 509 (1995).
[34] P. Smilauer, M. Wilby, and D. Vvedensky, Surf. Sci. **291**, L733 (1993).
[35] J. A. Venables, Surf. Sci. **299/300**, 798 (1994).
[36] H. Brune, H. Röder, C. Boragno, and K. Kern, Phys. Rev. Lett. **73**, 1955 (1994).
[37] R. Ferrando and G. Treglia, Phys. Rev. B **50**, 12 104 (1994).
[38] H. Röder, K. Bromann, H. Brune, and K. Kern, Surf. Sci. **376**, 13 (1997).
[39] The STM image that compares to our calculations is available at http://ipent.epfl.ch/gr_kern/kern.welcome.html
[40] M. Bott, M. Hohage, M. Morgenstern, T. Michely, and G. Comsa, Phys. Rev. Lett. **76**, 1304 (1996).